Molecular layer deposition of an Al-based hybrid resist for electron-beam and EUV lithography

Ajay Ravi[a], Jingwei Shi[b], Jacqueline Lewis[b], Stacey F. Bent[b]
[a]Department of Materials Science and Engineering, Stanford University, Stanford, CA 94305, USA;
[b]Department of Chemical Engineering, Stanford University, Stanford, CA 94305, USA

ABSTRACT

As lithographic techniques advance in their capabilities of shrinking microelectronics devices, the need for improved resist materials, especially for extreme ultraviolet (EUV), has become increasingly pressing. In this work, we study the molecular layer deposition (MLD) of an Al-based hybrid thin film resist, known as "alucone," extending our previous research that tested the Hf-based hybrid thin film "hafnicone" as an EUV resist. Alucone is grown at 100 ºC using the metal precursor trimethylaluminum and the organic precursor ethylene glycol. Like hafnicone, alucone behaves as a negative tone resist that can resolve 50-nm line widths, though preliminary data suggest that alucone's line patterns are more sharply defined than those of hafnicone. Whereas hafnicone's sensitivity is 400 μC/cm^2 using 3 M HCl as the developer, alucone's sensitivity is not yet as good (4800 μC/cm^2 using 0.125 M HCl). Our study of alucone offers new insight into structural features of an MLD film that can lead to desired EUV-responsive behavior. This insight may accelerate the development of vapor-deposited inorganic resists for use in electron-beam and EUV lithography.

Keywords: resists, thin films, extreme ultraviolet (EUV) lithography, molecular layer deposition (MLD), atomic layer deposition (ALD), hybrid organic-inorganic materials

1. INTRODUCTION

To ensure the extension of Moore's law, the microelectronics industry must continue to develop more advanced patterning techniques and processes. Deep ultraviolet (DUV) lithography (at 193 nm) remains the prevailing technique in large-scale industrial applications, but to reduce feature sizes without relying on multiple expensive and error-prone patterning techniques, the use of shorter wavelengths is necessary.[1-3] By generating smaller features, one can create denser integrated circuits to improve the energy efficiency of devices.[1-3] Extreme ultraviolet (EUV) lithography holds great potential in unlocking these benefits by using a significantly shorter wavelength (13.5 nm) than DUV lithography.[2] Yet, EUV lithography faces a cost-effectiveness problem toward its widespread industrial adoption.[1-3] Conventional resist materials are polymeric, consisting of C, H, and O, which are all weak EUV absorbers.[3] As a result, these materials require large EUV doses to cause a solubility change, i.e., they display poor sensitivity, preventing EUV lithography from offering high throughput.[3]

One strategy to overcome this problem is to incorporate a metal with a high EUV absorption cross-section into the resist material, yielding a hybrid organic-inorganic photoresist with superior sensitivity.[4-9] Hybrid photoresists are usually spin-coated, taking the form of inorganic nanoparticles (e.g., zinc oxide) surrounded by organic ligands (e.g., methacrylic acid).[10-15] Such materials are compositionally similar to hybrid thin films synthesized using molecular layer deposition (MLD), which are coordination polymers in which metal ions are linked by organic ligands.[16] While MLD and spin coating can both deposit hybrid photoresists, the former has several advantages over the latter. MLD can readily grow nanometer-scale photoresists with molecular-level thickness control, thus satisfying the need for thinner resists brought on by the decreased depth of focus in high numerical aperture (NA) EUV lithography.[16] This layer-by-layer technique also provides tunability over the film's chemical composition—and, by extension, its resist properties—by making it possible to synthesize films containing several distinct metal ions or ligands.[16] Despite these advantages, few MLD coordination polymers have been tested as EUV resists, so there is a limited understanding of how the MLD film structure affects its EUV response.[16-17]

In this work, we investigate the use of the MLD-grown hybrid alucone—comprised of Al atoms connected by ethylene glycol ligands—as an electron-beam and EUV resist. This work builds upon our group's earlier research on the resist performance and patterning mechanism of hafnicone, which differs from alucone only in its metal center. We evaluate

alucone's development characteristics, sensitivity, and resolution. Additionally, we compare these electron-beam resist properties to those of hafnicone. We use electron-beam lithography as a proxy for EUV exposure, since it is hypothesized that the resist's solubility change during EUV irradiation is due to secondary electrons.[16, 18] Ultimately, this study develops new understanding of how varying the metal ion (while keeping the organic linker unchanged) in the MLD hybrid film affects EUV- and electron-resist interactions.

2. EXPERIMENTAL SECTION

2.1 Reagents

Alucone films were synthesized using trimethylaluminum (TMA; Sigma-Aldrich) and anhydrous ethylene glycol (EG; Sigma-Aldrich). TMA and EG were used as received; the former was stored in a glovebox. Films were grown on single-sided, n-doped Si (100) substrates (WRS Materials). Before use, silicon wafers were sonicated in deionized water for 5 min, dried with compressed air, and cleaned for 15 min in a Novascan PSD Series Digital UV Ozone System to remove remaining organic contaminants.

2.2 Molecular layer deposition

Films were deposited in a custom-built, hot-walled tube reactor described previously.[16] This reactor was maintained at low vacuum with a Leybold Trivac rotary vane pump, and its body was held at 100 ºC for all depositions. The transfer lines and bubblers containing EG and TMA were held at 50 ºC and room temperature, respectively. Depositions were carried out for 100 MLD cycles, with each of these cycles divided into two half-cycles, where TMA was introduced in the first and EG in the second. Half-cycles were carried out with the following steps: (1) a predose pump time, in which the vacuum pump was kept open in the absence of nitrogen flow; (2) a dose time, in which the precursor valve was opened with 10 sccm of N_2 flowing and continued vacuum pumping; (3) a soak time, in which the precursor valve, the N_2 valve, and pump line were closed; and (4) a purge time, in which only the N_2 and the pump lines were reopened. For both half-cycles, the predose pump time was 15 s, and the soak time was 10 s. The dose and purge times for TMA were 1.2 s and 120 s, respectively, while those for EG were 1.5 s and 240 s.

2.3 Electron-beam lithography

The as-deposited alucone films were patterned using a Raith VOYAGER electron-beam lithography tool at 50 keV and 5 nA. Following exposure, films were developed using 0.125 M HCl for 2 min.

2.4 Deep ultraviolet lithography

To find a suitable developer for alucone, DUV blanket exposures were performed on as-deposited films. These exposures were done in ambient with a 254 nm DUV lamp (Cole-Parmer, reported intensity of 280 $\mu W/cm^2$) for 5 hr, corresponding to doses of 5000 mJ/cm^2.[16]

2.5 Resist characterization

Film thicknesses were measured using a J. A. Woollam Co. α-SE spectroscopic ellipsometer with a spectral range of 300–900 nm. To determine films' surface elemental composition and bonding environment, X-ray photoelectron spectra were acquired using a PHI Versaprobe 4 with a monochromatic Al Kα X-ray source (1486 eV). Survey spectra were obtained at a pass energy of 224 eV, and high-resolution spectra were collected at a pass energy of 55 eV. To further probe bonding in the films, Fourier transform infrared (FTIR) spectroscopy was completed with a Nicolet iS50 FTIR spectrometer (ThermoFisher Scientific) with a Harrick VariGATR accessory attached. Using a HgCdTe detector, FTIR spectra were collected with 64 scans over a scan range of 650 to 4000 cm^{-1}. Film morphology post-exposure and development was imaged using the Apreo S LoVac Scanning Electron Microscope at an acceleration voltage of 2 kV. The thicknesses of exposed and developed patterns were found using a Bruker Pektak XT-A profilometer with a 1 mg force probe.

3. RESULTS AND DISCUSSION

3.1 Molecular layer deposition of alucone films

Alucone films were deposited for 100 cycles, achieving a thickness of 279 ± 32 Å, (mean ± standard deviation), which corresponds to a growth per cycle (GPC) of 2.8 Å/cycle. This GPC is slightly greater than that reported by George et al. (2.6 Å/cycle), although these values fall within the uncertainty of the measurement.[19] The differing GPC values might be attributed to the higher reactor stage temperature used by George et al., which was 105 ºC rather than 100 ºC.[19] For alucone MLD, it has been observed that GPC decreases as deposition temperature increases.[19]

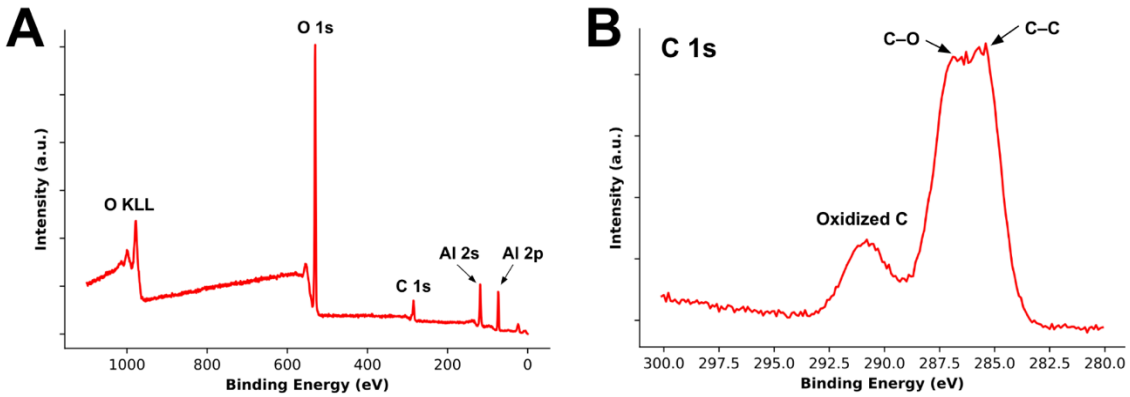

Figure 1. (A) X-ray photoelectron spectroscopy (XPS) survey spectrum of an alucone film revealing the expected elements: C, Al, and O. (B) XPS C 1s high-resolution spectrum of alucone, which suggests the expected presence of C–O bonding.

The XPS survey scan shown in Figure 1A indicates the presence of the expected elements in the alucone film: Al, C, and O. However, these elements do not appear in the ideal ratio for alucone, whose stoichiometry is given by $Al(CH_2O)_3$. Rather than displaying the ideal 3:3:1 ratio of C:O:Al, the as-deposited film showed a 0.9:3.8:1 ratio, as determined by XPS. The film measured by XPS is thus carbon deficient. One possible explanation for this compositional difference is that the film was exposed in ambient conditions for around 30 minutes before XPS characterization. During these 30 minutes, alucone likely reacted with water to form some Al_2O_3, increasing the film's oxygen content.[19] Another potential explanation is that the ethylene glycol bubbler, which was filled in ambient, may have contained some water, which would result in the deposition of an alucone-Al_2O_3 mixture instead of pure alucone.

The deviation in the film from alucone's ideal stoichiometry prompted us to additionally probe the bonding via XPS and IR spectroscopy. The C1s high-resolution spectrum (Figure 1B) shows three peaks at roughly 285, 286, and 291 eV. We assign the first peak to carbon bonded to other carbon (C–C) and the last peak to oxidized carbon species. The middle peak, assigned to single C-O bonding, suggests that the as-deposited film contain the C–O bonds expected for alucone.[16]

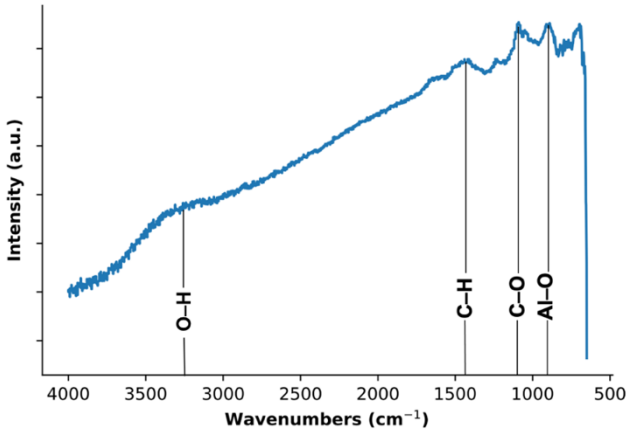

Figure 2. FTIR spectrum of alucone, which displays the expected C–H, C–O, Al–O vibrational modes.

Corroborating this result, the infrared spectrum for as-deposited alucone (Figure 2) shows a C–O stretch at 1090 cm^{-1}.[19] The two adjacent peaks at 1439 and 889 cm^{-1} correspond to the expected C–H deformation and Al–O stretching vibrational modes, respectively.[16, 19] The broad peak near 3200 cm^{-1} is assigned to an O–H stretching vibrational mode, which likely arises as a result of water absorption in the alucone film.[19]

3.2 Evaluating resist properties of alucone films

Once deposited, the alucone films were patterned using electron-beam lithography to evaluate their resist properties. Such patterning experiments required us to first identify a suitable developer for these films, i.e., a solvent in which they will switch solubility upon exposure.

We searched for a developer that would remove the as-deposited film, because we hypothesized that alucone would work as a negative-tone resist. This hypothesis was grounded in our previous work which demonstrated that hafnicone exhibited negative resist behavior. The negative resist mechanism for hafnicone was proposed as follows: irradiation causes cleavage of the C–O bond in ethylene glycol linkers, which then enables the agglomeration of hafnium oxide nanoparticles that are insoluble in the developer (3 M HCl).[16] Given that hafnicone and alucone are compositionally similar, we anticipated that alucone's patterning mechanism would likewise entail bond cleavage followed by aluminum oxide nanoparticle agglomeration. Since Al_2O_3 is insoluble in most solvents, we aimed to find a solvent that would dissolve unexposed (rather than exposed) alucone.

A number of potential developers were tested by immersing unexposed alucone films in organic solvents, acids, and deionized water and then measuring their post-development thicknesses using ellipsometry. The results of the development testing are depicted in Figure 3, in which normalized thickness (defined as post-development thickness divided by as-deposited thickness) is plotted against development time. As Figure 3 shows, only 1 M HCl removed unexposed alucone. For comparison, our earlier work tested the same solvents with as-deposited hafnicone and similarly reported that HCl was the only one that reduced its normalized thickness to zero.[16]

After completing the development experiments, we optimized the HCl concentration by performing photon flood exposures on alucone using a DUV lamp at a dose of 5000 mJ/cm^2. We ultimately determined the concentration (0.125 M) that maximized the thickness difference between exposed and unexposed alucone.

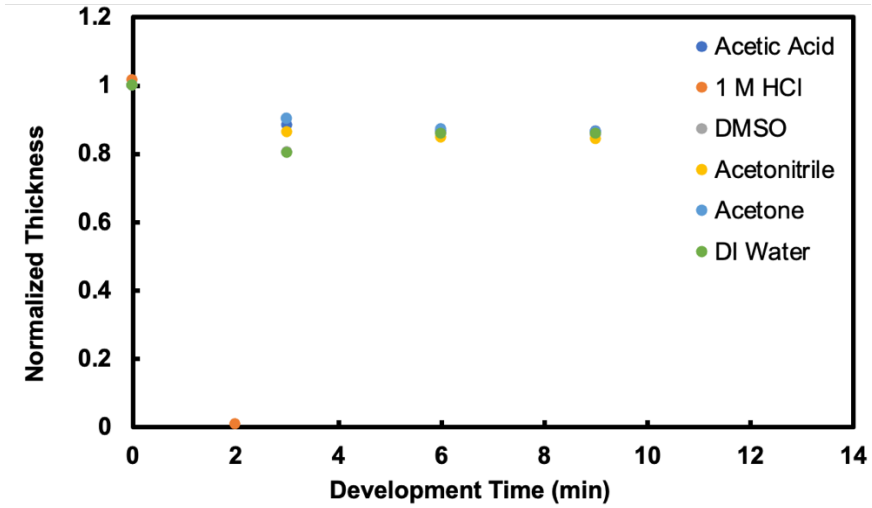

Figure 3. Development plot for as-deposited alucone, where normalized thickness is defined as post-development thickness divided by as-deposited thickness. The normalized thickness of alucone goes to zero upon immersion in 1 M HCl but not in any of the other solvents tested. The data marker for 1 M HCl at 0 min development time is slightly offset from its value of 1.0 for ease of viewing.

With 0.125 M HCl as the developer, an electron-beam lithography experiment was performed to establish the sensitivity of the alucone film—that is, the threshold electron dose required to induce a solubility switch. Alucone was exposed to the dose matrix shown in Figure 4A, a rectangular array of squares corresponding to electron doses that linearly increased from 3000 to 10,200 $\mu C/cm^2$. The exposed material was then submerged in 0.125 M HCl for 2 min and finally imaged using scanning electron microscopy (SEM). Figure 4B displays the SEM image of the pattern after exposure and

development. The contrast observed in the SEM image suggests that the dose matrix pattern was successfully transferred.

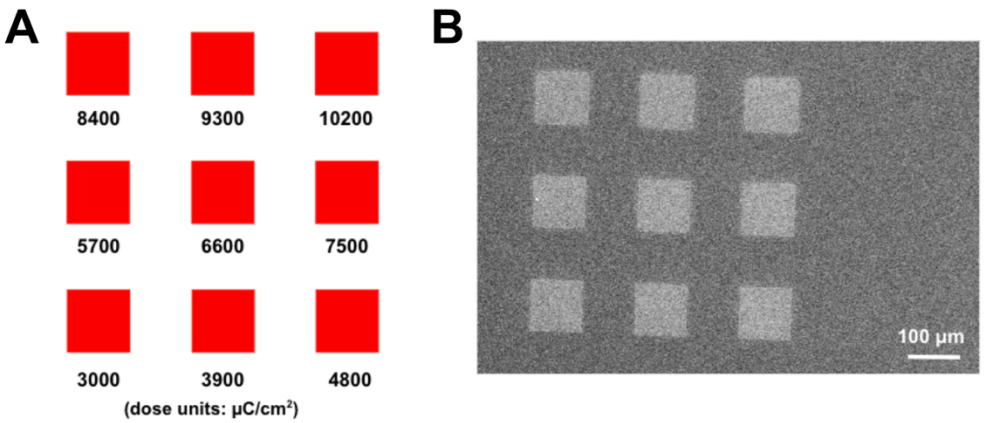

Figure 4. (A) Illustration of the electron dose matrix pattern, with the numbers under each square representing the electron dose in units of μC/cm^2. (B) SEM image of alucone after exposure to the dose matrix and development in 0.125 M HCl for 2 min.

The exposed and developed dose matrix was scanned using a profilometer to construct the sensitivity plot presented in Figure 5. This plot displays the exposed and developed thickness, normalized by alucone's as-deposited thickness, as a function of logarithmic exposure dose. According to Figure 5, alucone's sensitivity is around 4800 μC/cm^2, as the normalized thickness plateaus past this point. Notice that even above the sensitivity dose, the normalized thickness never reaches a value of 1. This observation is consistent with our earlier results for hafnicone, which revealed that its post-exposure thickness was roughly 67% of its as-deposited thickness, likely because of hafnicone's irradiation-induced conversion to hafnia and resulting shrinkage of the film.[16] Similarly, we anticipate that alucone's normalized thickness will be below 1 due to alucone's conversion to alumina during exposure.

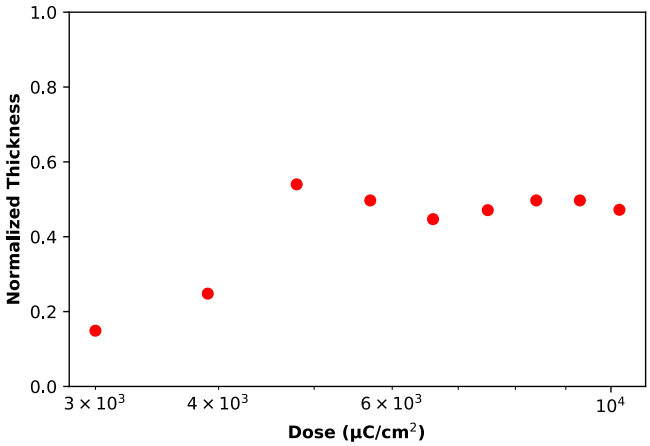

Figure 5. Sensitivity curve of the alucone film, with normalized thickness defined as post-exposure and -development thickness divided by as-deposited thickness. This curve indicates that alucone's sensitivity is roughly 4800 μC/cm^2, as normalized thickness begins to plateau around that dose.

Comparing the alucone results with those of hafnicone, it is clear that hafnicone's sensitivity (400 μC/cm^2) is lower by an order of magnitude.[16] We hypothesize that there are several factors that might explain the difference: coordination

bond strength, surface energy of the metal oxide nanoparticle, and nanoparticle diffusivity. Further study will be performed to help identify the origin of the difference.

We next performed a box-and-grating experiment to test the resolution of the alucone film, i.e., the narrowest line pattern that the material could resolve. The film was exposed to the pattern displayed in Figure 6A, which contains line widths that progressively decrease from 500 to 5 nm at two different line pitches, 100 nm and 50 nm. Subsequently, the exposed material was developed in 0.125 M HCl, again for 2 min. Figure 6B shows an SEM image of the exposed and developed box-and-grating pattern, revealing that sub-50 nm line widths can be resolved in the alucone resist. For alucone, the lines narrower than 50 nm are sharper than those previously reported for hafnicone.[16]

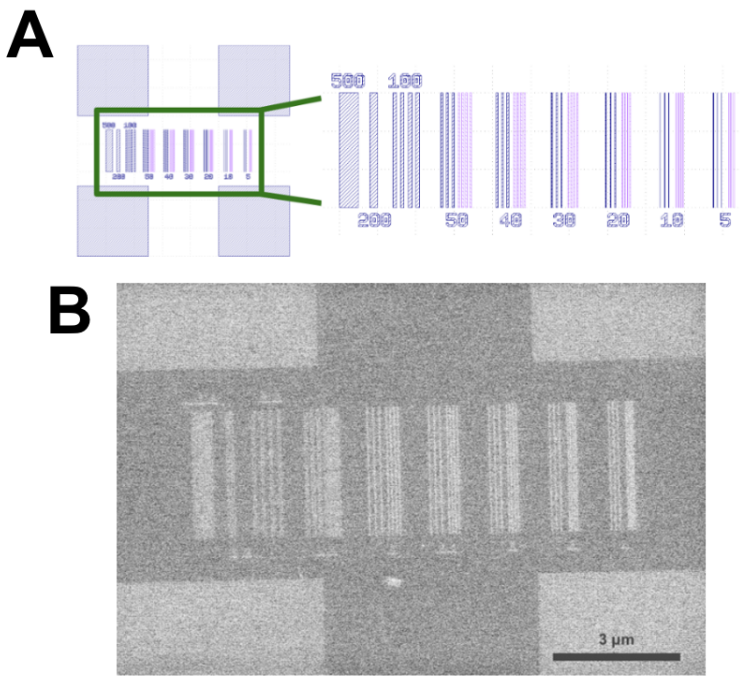

Figure 6. (A) Box and grating pattern, in which lines were spaced 100 nm (blue) and 50 nm (purple) apart. The line widths (in nm) are written under the gratings, ranging from 500 to 5 nm. (B) SEM image of alucone, following exposure to the box and grating pattern and development in 0.125 M HCl.

CONCLUSION

We have demonstrated that the MLD hybrid film alucone, like hafnicone, can work as a negative-tone resist for EUV lithography, using electron-beam lithography as a proxy. Our results have confirmed the chemical composition, bonding, and thickness of as-deposited alucone using XPS, IR spectroscopy, and ellipsometry. The solvent in which alucone exhibits a solubility switch upon irradiation was found to be 0.125 M HCl, a substantially less aggressive developer than that required for hafnicone (3 M HCl). On the other hand, alucone's solubility switch requires a minimum electron dose of 4800 $\mu C/cm^2$, an order of magnitude greater than hafnicone's sensitivity of 400 $\mu C/cm^2$. At the same time, preliminary results indicate that alucone shows significantly sharper line widths than hafnicone when exposed to a box-and-grating pattern. Future work will probe the origin of these differences in resist performance between alucone and hafnicone. This study therefore contributes to a better fundamental understanding of the metal atom's role in determining the irradiation-responsiveness an MLD hybrid film. Such understanding can lay the groundwork for future optimization of resist properties, particularly sensitivity and resolution, and ultimately advance the trend toward smaller microelectronic devices.

ACKNOWLEDGEMENTS

Alucone MLD process development and preliminary resist testing was supported by the National Science Foundation (Grant CHE-1904108). Part of this work was performed at the Stanford Nano Shared Facilities (SNSF), supported by the National Science Foundation under award ECCS-2026822.

REFERENCES

[1] Gao, P., Li, X., Zhao, Z., Ma, X., Pu, M., Wang, C., and Luo, X., "Pushing the plasmonic imaging nanolithography to nano-manufacturing," Opt. Commun. 404, 62-72 (2017).

[2] Wu, L., Bespalov, I., Witte, K., Lugier, O., Haitjema, J., Vockenhuber, M., Ekinci, Y., Watts, B., Brouwer, A. M., and Castellanos, S., "Unravelling the effect of fluorinated ligands in hybrid EUV photoresists by X-ray spectroscopy," J. Mater. Chem. C 8, 14757-14765 (2020).

[3] Closser, K. D., Ogletree, D. F., Naulleau, P., and Prendergast, D., "The importance of inner-shell electronic structure for enhancing the EUV absorption of photoresist materials," J. Chem. Phys. 146, 164106 (2017).

[4] Luo, C., Xu, C., Lv, L., Li, H., Huang, X., and Liu, W., "Review of recent advances in inorganic photoresists," RSC Adv. 10, 8385-8395 (2020).

[5] Krysak, M., Trikeriotis, M., Schwartz, E., Lafferty, N., Xie, P., Smith, B., Zimmerman, P., Montgomery, W., Giannelis, E., and Ober, C. K., "Development of an inorganic nanoparticle photoresist for EUV, e-beam, and 193nm lithography," Adv. Resist Mater. Process. Technol. XXVIII 7972, 79721C (2011).

[6] Trikeriotis, M., Krysak, M., Chung, Y. S., Ouyang, C., Cardineau, B., Brainard, R., Ober, C. K., Giannelis, E. P., and Cho, K., "A new inorganic EUV resist with high-etch resistance," Extrem. Ultrav. Lithogr. III 8322, 83220U (2012).

[7] Thakur, N., Tseng, L.-T., Vockenhuber, M., Ekinci, Y., and Castellanos, S., "Stability studies on a sensitive EUV photoresist based on zinc metal oxoclusters," J. Micro/Nanolithography, MEMS, MOEMS 18, 1 (2019).

[8] Thrun, X., Choi, K.-H., Freitag, M., Grenville, A., Gutsch, M., Hohle, C., Stowers, J. K., Bartha, J. W., Toriumi, M., Sato, Y., Koshino, M., Suenaga, K., Itani, T., Kumai, R., Yamashita, Y., Tsukiyama, K., Itani, T., Thakur, N., Tseng, L.-T., Vockenhuber, M., Ekinci, Y., Castellanos, S., Luo, C., Xu, C., Lv, L., Li, H., Huang, X., Liu, W., Toriumi, M., Sato, Y., Koshino, M., Suenaga, K., and Itani, T., "Metal resist for extreme ultraviolet lithography characterized by scanning transmission electron microscopy," Appl. Phys. Express 9, 97790G (2016).

[9] Toriumi, M., Sato, Y., Koshino, M., Suenaga, K., and Itani, T., "Metal resist for extreme ultraviolet lithography characterized by scanning transmission electron microscopy," Appl. Phys. Express 9, 031601 (2016).

[10] Li, L., Chakrabarty, S., Spyrou, K., Ober, C. K., Giannelis, E. P., "Studying the mechanism of hybrid nanoparticle photoresists: effect of particle size on photopatterning," Chem. Mater. 27, 5027-5031 (2015).

[11] Saifullah, M. S. M., Khan, M. Z. R., Hasko, D. G., Leong, E. S. P., Neo, X. L., Goh, E. T. L., Anderson, D., Jones, G. A. C., and Welland, M. E., "Spin-coatable HfO2 resist for optical and electron beam lithographies," J. Vac. Sci. Technol. B, Nanotechnol. Microelectron. Mater. Process. Meas. Phenom. 28, 90-95 (2010).

[12] Stowers, J. K., Telecky, A., Kocsis, M., Clark, B. L., Keszler, D. A., Grenville, A., Anderson, C. N., and Naulleau, P. P., "Directly patterned inorganic hardmask for EUV lithography," Extrem. Ultrav. Lithogr. II 7969, 796915 (2011).

[13] Oleksak, R. P., Ruther, R. E., Luo, F., Fairley, K. C., Decker, S. R., Stickle, W. F., Johnson, D. W., Garfunkel, E. L., Herman, G. S., and Keszler, D. A., "Chemical and structural investigation of high-resolution patterning with HafSOx," ACS Appl. Mater. Interfaces 6, 2917-2921 (2014).

[14] Toriumi, M., Sato, Y., Kumai, R., Yamashita, Y., Tsukiyama, K., and Itani, T., "Characterization of 'metal resist' for EUV lithography," Adv. Patterning Mater. Process. XXXIII 9979, 99790G (2016).

[15] Sakai, K., Xu, H., Kosma, V., Giannelis, E. P., and Ober, C. K., "Progress in metal organic cluster EUV photoresists," J. Vac. Sci. Technol. B 36, 06J504 (2018).

[16] Shi, J., Ravi, A., Richey, N. E., Gong, H., and Bent, S. F., "Molecular layer deposition of a hafnium-based hybrid thin film as an electron beam resist," ACS Appl. Mater. Interfaces 14, 27140-27148 (2022).

[17] Le, D. N., Hwang, S. M., Woo, J., Choi, S., Park, T., Veyan, J.-F., Tiwale, N., Subramanian, A., Lee, W.-I., Nam, C.-Y., Choi, R., and Kim, J., "Chemical reactions induced by low-energy electron exposure on a novel inorganic-organic hybrid dry EUV photoresist deposited by molecular atomic layer deposition (MALD)," Proc. SPIE 12292, 1229205 (2022).

[18] Pollentier, I., Vesters, Y., Jiang, J., Vanelderen, P., and De Simone, D., "Unraveling the role of secondary electrons upon their interaction with photoresist during EUV exposure," Proc. SPIE 10450, 17 (2017).
[19] Dameron, A. A., Seghete, D., Burton, B. B., Davidson, S. D., Cavanagh, A. S., Bertrand, J. A., and George, S. M., "Molecular layer deposition of alucone polymer films using trimethylaluminum and ethylene glycol," Chem. Mater. 20, 3315-3326 (2008).
[20] Tavakoli, A. H., Maram, P. S., Widgeon, S. J., Rufner, J., Benthem, K., Ushakov, S., Sen, S., and Navrotsky, A., "Amorphous alumina nanoparticles: structure, surface energy, and thermodynamic phase stability," J. Phys. Chem. C 117, 17123-17130 (2013).
[21] Sharma, G., Ushakov, S. V., Li, H., Castro, R. H. R., and Navrotsky, A., "Calorimetric measurements of surface energy of amorphous HfO2 nanoparticles produced by gas phase condensation," J. Phys. Chem. C 121, 10392-10397 (2017).